Inhibition of neural crest migration underlies craniofacial dysmorphology and Hirschsprung's disease in Bardet–Biedl syndrome

Jonathan L. Tobin*, Matt Di Franco†, Erica Eichers‡, Helen May-Simera*, Monica Garcia‡, Jiong Yan‡, Robyn Quinlan*, Monica J. Justice‡, Raoul C. Hennekam§¶, James Briscoe‖, Masazumi Tada**, Roberto Mayor**, Alan J. Burns††, James R. Lupski‡, Peter Hammond*†, and Philip L. Beales*‡‡

*Molecular Medicine Unit, UCL Institute of Child Health, 30 Guilford Street, London WC1N 1EH, United Kingdom; †Biomedical Informatics Unit, UCL Eastman Dental Institute for Oral Health Care Sciences, 256 Gray's Inn Road, London WC1X 8LD, United Kingdom; ‡Department of Molecular and Human Genetics, Baylor College of Medicine, One Baylor Plaza, Houston, TX 77030; ‖Developmental Neurobiology, National Institute for Medical Research, London NW7 1AA, United Kingdom; **Department of Anatomy and Developmental Biology, University College London, London WC1E 6BT, United Kingdom; ††Neural Development Unit, UCL Institute of Child Health, 30 Guilford Street, London WC1N 1EH, United Kingdom; §Clinical and Molecular Genetics Unit, UCL Institute of Child Health, 30 Guilford Street, London WC1N 1EH, United Kingdom; and ¶Department of Pediatrics, Academic Medical Centre, University of Amsterdam, 1105 AZ Amsterdam, The Netherlands

Edited by Kathryn V. Anderson, Sloan–Kettering Institute, New York, NY, and approved March 6, 2008 (received for review July 30, 2007)

Facial recognition is central to the diagnosis of many syndromes, and craniofacial patterns may reflect common etiologies. In the pleiotropic Bardet–Biedl syndrome (BBS), a primary ciliopathy with intraflagellar transport dysfunction, patients have a characteristic facial "gestalt" that dysmorphologists have found difficult to characterize. Here, we use dense surface modeling (DSM) to reveal that BBS patients and mouse mutants have mid-facial defects involving homologous neural crest-derived structures shared by zebrafish morphants. These defects of the craniofacial (CF) skeleton arise from aberrant cranial neural crest cell (NCC) migration. These effects are not confined to the craniofacial region, but vagal-derived NCCs fail to populate the enteric nervous system, culminating in disordered gut motility. Furthermore, morphants display hallmarks of disrupted Sonic Hedgehog (Shh) signaling from which NCCs take positional cues. We propose a model whereby Bbs proteins modulate NCC migration, contributing to craniofacial morphogenesis and development of the enteric nervous system. These migration defects also explain the association of Hirschsprung's disease (HD) with BBS. Moreover, this is a previously undescribed method of using characterization of facial dysmorphology as a basis for investigating the pathomechanism of CF development in dysmorphic syndromes.

sonic hedgehog | Wnt | cilia | cell migration

Recognition of the facial "gestalt" is central to diagnosis of many genetic disorders, but the great variability of features often hinders successful classification (1). Recently, noninvasive 3D surface imaging has characterized dysmorphology in syndromes (2, 3). None, however, has been used to either define subtle facial dysmorphism or aid investigation of mechanisms for craniofacial dysmorphology.

Bardet–Biedl syndrome (BBS) causes retinal degeneration, postaxial polydactyly, obesity, renal dysfunction, and cognitive impairment. Twelve BBS genes (*BBS1–BBS12*) have been discovered, and pathogenesis lies in primary cilia dysfunction (4). BBS4, BBS6, and BBS8 (investigated in this study) are expressed in ciliated epithelia and localize to the centrosome and basal bodies of ciliated cells (5–7). Subtle craniofacial abnormalities in patients have been reported (8–10). Among the many additional features of BBS is Hirschsprung's disease (HD), a disorder of the enteric nervous system (ENS) (11).

Streams of neural crest cells (NCCs) from the caudal brain form most of the craniofacial (CF) skeleton (see ref. 12 for review). Cranial NCCs (CNCC) follow defined paths to populate the frontonasal prominence and branchial arch mesenchyme. Here, they proliferate and differentiate into structures of the face and cranium. Sonic Hedgehog (Shh) expressed in the ventral brain and oral ectoderm is essential for the formation of most facial structures (12). Shh-deficient mice have severe loss of craniofacial bones, and, in humans, *SHH* mutations cause midline CF defects with holoprosencephaly (HPE) (12).

The ENS regulates gastrointestinal motility and secretion. It derives from vagal and lumbosacral NCCs (13). In HD, characterized by megacolon, there are reduced or absent enteric ganglia in the distal colon.

Despite the plethora of recent evidence pointing to ciliary dysfunction in BBS, both craniofacial and gastrointestinal defects are difficult to reconcile on this basis alone. In this study, we show that BBS proteins are required for NCC migration, culminating in Shh-dependent craniofacial defects, and gut motility disorder, likely underlying the HD association with BBS.

Results

Three-Dimensional Dense Surface Modeling (DSM) Reveals Comparable Craniofacial Defects in Man and Mouse. To assess CF defects in BBS, we performed 3D DSM face analysis on 83 patients (irrespective of mutations) and 230 controls. To account for growth differences, analyses were performed separately for subjects <20 years old. Facial scans were annotated with key landmarks [supporting information (SI) Fig. S1], DSMs of facial and nasal regions were computed for subsets of faces, and differences between control and BBS landmarks were measured. Of several interlandmark measurements, the most significant were anomalous length and width of the face (Fig. S2). To avoid the effects of excessive soft tissue in patient faces, we first restricted shape analysis to the nasal region where obesity has least effect. Color-distance-coded comparisons of mean BBS and control noses for children and adults showed nasal bridge hypoplasia and nasal shortening/reduced bulbosity at the nasal tip (red-yellow; Fig. 1 *A* and *B*). Dynamic morphs between BBS and control mean noses demonstrate these and other shape differences in the nasal alae and

Author contributions: J.L.T., J.B., R.M., A.J.B., J.R.L., P.H., and P.L.B. designed research; J.L.T., M.D.F., E.E., H.M.-S., M.G., J.Y., R.Q., M.J.J., R.C.H., M.T., A.J.B., and P.H. performed research; H.M.-S., J.B., M.T., R.M., and A.J.B. contributed new reagents/analytic tools; J.L.T., M.D.F., M.J.J., A.J.B., J.R.L., P.H., and P.L.B. analyzed data; and J.L.T., P.H., and P.L.B. wrote the paper.

The authors declare no conflict of interest.

This article is a PNAS Direct Submission.

Freely available online through the PNAS open access option.

‡‡To whom correspondence should be addressed. E-mail: p.beales@ucl.ac.uk.

This article contains supporting information online at www.pnas.org/cgi/content/full/0707057105/DCSupplemental.

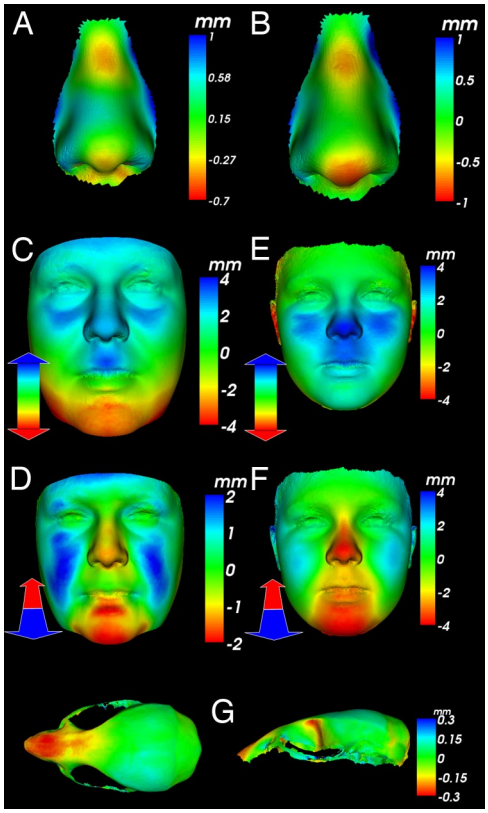

Fig. 1. Color-distance-coded mean morphology of BBS patients (nose and face) and *Bbs6* mutant mice (dry skulls) compared with WT controls. (*A* and *B*) Comparison normal to surface for BBS children (*A*)/adults (*B*) with red-yellow patches showing hypoplasia at nasal bridge and reduced length/bulbosity at nasal tip. (*C*) Vertical comparison for male adult patients with blue patch showing mid-facial shortening. (*D*) Depth-wise for female adult patients with red-yellow region showing mid-facial flattening and mild retrognathia. (*E*) Vertical comparison for BBS children with blue patch showing mid-facial shortening. (*F*) Depth-wise comparison for BBS children with red-yellow region showing mid-facial flattening and mild retrognathia. (*G*) Normal to surface for Bbs6 mice with red-yellow region showing reduction in premaxillary and maxillary regions (note: mandibles were removed before imaging). (*Left*) Dorasl view. (*Right*) Lateral view.

columella (see Movies S1 and S2). Multifolded testing using pattern recognition algorithms established significant discrimination [receiver-operator characteristic (ROC) analysis], using nose shape alone (Table S1). In adult patients, color-distance-coded comparisons of mean face shape with that of controls demonstrated relative upward displacement of the nose and upper lip (blue regions in Fig. 1*C*), mid-facial hypoplasia and mild retrognathia (red-yellow regions of Fig. 1*D*).

Principal component 3 of the DSM for control children reflected flatness of the mid-face, and mandible retrusion was strongly correlated [Pearson product moment correlation (PPMC) = 0.81] with the classification position of a face with respect to the mean control and BBS children's faces (Fig. S3). An age/size-adjusted comparison of the mean affected BBS and control children's faces demonstrated greater face width and upward nasal displacement (Fig. 1*E*), as well as mid-facial flattening and retrognathia (Fig. 1*F*). Our results indicate that this technique can distinguish subtle facial phenotypes that challenge even experienced dysmorphologists.

We next investigated whether mouse BBS models (*Bbs4*$^{-/-}$ and *Bbs6*$^{-/-}$) might have similar craniofacial malformations. *Bbs4*$^{-/-}$ ($n = 31$), heterozygous ($n = 30$), and WT ($n = 20$) mice were imaged by using a 3D laser scanner (Fig. S2). Despite gross differences in craniofacial anatomy between humans and mice, there were significant similarities in key ratios, including a larger mid-face width to height ($P < 0.01$), and a shorter snout ($P < 0.01$). Similar surface abnormalities were seen in *Bbs6*-null mice (Table S2). Heterozygotes showed no landmark anomalies.

To determine the detailed bony origins of the craniofacial changes, we next 3D laser surface-scanned *Bbs6*$^{-/-}$ ($n = 9$) and WT ($n = 15$) skulls. Color-coded comparisons of the mean skull surfaces confirm that shortening is attributable to premaxillary and maxillary hypoplasia, resulting in a significantly shorter snout, similar to human deficits (Fig. 1 *F* and *G* and Movie S3).

Zebrafish *bbs* Morphants Have Craniofacial Defects Mirroring Mammalian Mutants. Despite morphological differences between mammalian and fish skulls, many of the same signaling molecules regulate their development, and the organization of the cranial skeleton is remarkably similar (12). The anterior neurocranium (ANC) consists of the trabeculae and the ethmoid plate, both of which are NC derived and analogous to the mammalian maxilla (14).

To assess the etiology of the human and mouse CF defects, we injected zebrafish embryos with *bbs4*, *bbs6*, and *bbs8* morpholinos (MO) and visualized cranial cartilages at 5 days postfertilization (dpf). Despite a convergent-extension (CE) defect (15, 16), *bbs4* morphants had largely normal CF morphology (Fig. 2 *B*, *G*, and *L* and *A*, *F*, and *K*) although the mandibles were wider and shorter. In *bbs6* morphants, the ANC was shortened, compressing the face (Table S3). The mandibles were greatly reduced, and there were fewer hypoplastic branchial arches (Fig. 2 *C*, *H*, and *M*). *bbs8* is widely expressed in the zebrafish embryo (Fig. S4).

The most severe defects were consistently observed with the *bbs8* MO: depigmentation, partial cyclopia, and craniofacial reduction in which the ANC was shortened with midline fusion of the trabeculae (Fig. 2 *D*, *I*, and *N*). In ≈20% of cases, cartilage was completely absent in the head (Fig. 2*D Inset*). Mandibles and branchial arches were completely absent at 5 dpf (Fig. 2*D*), and Sox10 expression at 72 hpf (see Fig. S5*A*) showed these failed to form. Coinjections with human *bbs8* mRNA rescued these defects completely (Fig. 2 *E*, *J*, and *O*), as did *bbs4* and *bbs6* mRNA (data not shown). By calculating the ratio between ANC and body length, we showed that the shortened ANC is independent of CE defects (Fig. S6*A*).

NCC Migration Underlies the Craniofacial Phenotype in Zebrafish. The majority of the head skeleton derives from the CNCC, from which cells migrate in a stereotypic fashion to the branchial arches and frontonasal process. To see whether Bbs proteins were involved in NCC migration and CF morphogenesis, we investigated three key stages in early NCC development: specification, maintenance, and migration in the *bbs* morphants. Expression of *foxd3* and *sox10* were normal at 5-somite stage (ss), proving that specification was unaltered (Fig. S7). At 12ss, expression of *crestin* signified that NCC maintenance was normal (Fig. S7).

However, at 20ss, streams of *crestin*-expressing NCCs that normally migrate ventrally from the neural tube (NT) into the trunk were disrupted in *bbs* morphants. The degree of migration correlated with the level of CF defect (most severe in *bbs8* morphants) (Fig. 2 *P–S*). Quantification of migrating streams (Fig. 2*Y*) correlated directly with the decreasing ratio of neurocranial length to width in *bbs4*, *bbs6*, and *bbs8* morphants, respectively (Fig. S6*B*). To corroborate this *in situ* hybridization data, we observed a similar pattern of NCC migration using Sox10:eGFP zebrafish, which express GFP in NCCs (gift of R. Kelsh) (Fig. 2 *U–X*) (14). Again, the *bbs8* phenotype was rescued with human mRNA (Fig. 2*T*). The abundance of NCCs in the NT suggests that induction, maintenance, or proliferation is unaffected; rather, there is an inhibition of cell migration.

In support of a suspected role for Bbs8 in NC development, the *bbs8* morphants, which have disrupted craniofacial morphology and almost no trunk NC migration, also lack melanocytes, another

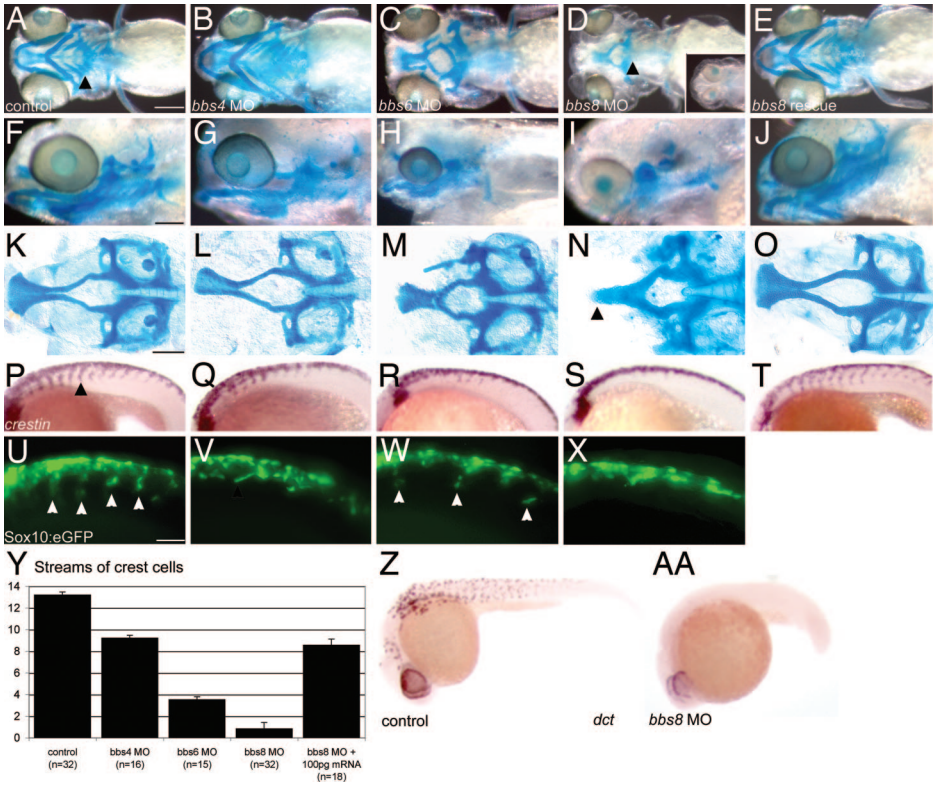

Fig. 2. Craniofacial and neural crest defects in *bbs* zebrafish morphants. (*A–E*) Ventral views of wholemount, Alcian Blue-stained, 5-dpf zebrafish. *bbs8* morphants are most severe (*D*), with loss of pharyngeal apparatus (2D arrowhead), mandibles, and shortening of the chondrocranium. (*F–J*) Lateral views of larvae showing reduction of branchial arches and shortening of the mandibles in *bbs6* and *bbs8* morphants. (*K–O*) Flatmounts of neurocrania of controls and morphants. *bbs8* morphants often have fusion of the trabeculae at the midline (arrowhead) similar to *syu* mutants. (*P–T*) *Crestin in situ* in 20ss embryos reveals streams of migrating NCCs in controls (arrowhead) with progressively fewer streams in *bbs4*, *bbs6*, and *bbs8* morphants, respectively. (*U–X*) Sox10:eGFP expression in migrating streams (arrowheads) shows a similar reduction in the number of streams to the *crestin* expression. (*Y*) Quantification of the number of streams in morphants confirms a severe neural crest migration defect in *bbs8* morphants that can be rescued by human mRNA. (*Z* and *AA*) *dct* expression in 27 hpf control embryos (*Z*) and *bbs8* morphants (*AA*). [Scale bars: 500 μm (*A–J*), 100 μm (*K–O*), and 100 μm (*P–X*).]

NC-derived lineage. There was no expression of *dct*, a marker of melanocyte precursors, in *bbs8* morphants at 27 hpf compared with controls (Fig. 2 *Z* and *AA*).

We chose to study the *bbs8* morphants further, using the Sox10:eGFP transgenic zebrafish. In controls at 12ss, NCCs have just begun to migrate from the region behind the eye into the head (Fig. 3*A*). By 20ss, the NCCs have migrated to the anterior-most region of the embryo, ≈250 μm (Fig. 3*B*). In *bbs8* morphants, migration failed to initiate by 12ss (Fig. 3*C*). By 20ss, the cells had only migrated midway through the eye, ≈80 μm (Fig. 3*D*).

To determine whether this migration disorder is cell autonomous or a consequence of adjacent tissue inhibition, we performed grafting experiments. Sox10:eGFP transgenic embryos were coinjected with a control or a *bbs8* MO. At 4 hpf, cells were transplanted from injected donors into control or morphant hosts. Successful transplants were imaged at 12ss for 4 h. Upon transplantation of control-MO injected cells into control hosts, NCCs migrated anteriorly ≈150 μm (Fig. 3 *E* and *E′*). However, *bbs8* morphant donor cells transplanted into control hosts failed to migrate, suggesting that loss of Bbs8 has a cell-autonomous role in inhibiting migration (Fig. 3 *F* and *F′*). Control donor cells transplanted into morphant hosts migrated normally, proving that migration inhibition is not secondary to tissue inhibition (Fig. 3 *G* and *G′*).

To exclude the possibility of a failure of early NC proliferation, we FACS sorted whole Sox10:eGFP control and morphant embryos at 16ss and 20ss. The proportion of NCCs in morphants was similar to controls at 20ss (4.4% vs. 4.7%, $P = 0.23$) (Fig. S6 *G* and *H*). We also excluded NC cell death as a causative factor, using 7AAD to quantify the number of dead Sox10-positive cells (0.5% controls vs. 0.7% morphants). In addition, using the mitotic marker PH3, we did not see any difference in proliferation of Sox10-positive cells at 24 hpf or 72 hpf in morphants (Fig. S5 *A–D*).

We next excluded the possibility of misdifferentiation of the NCCs. Although the morphant trunk NCCs remained in the NT, they did not inappropriately differentiate into neurons at 30 hpf (HuC/D)(Fig. S5 *E* and *F*).

At 48 hpf, we observed failure of extension of the primordial trabeculae and absence of the ethmoid plate in formation of the ANC in *bbs8* morphants in Sox10:eGFP embryos (Fig. 3 *H* and *I*), suggesting that the CF dysmorphology arises from reduction in early NCC migration, leading to a failure of cells to populate the ethmoid plate.

High-power imaging of the CNCCs migrating anteriorly around the eye shows cell protrusions mainly polarized in the direction of migration in controls at 12ss (Fig. 3*J*). In *bbs8* morphants, these cells were tightly clustered and lacked the protrusions seen on control cells (Fig. 3*K*).

Next, we examined the actin cytoskeleton in migrating CNCCs, NIH 3T3, and primary fibroblasts from *BBS8* patients. Despite difficulties in resolving the cytoskeleton of CNCCs *in vivo*, we observed disorganized microfilaments in morphants (data not shown). A mispolarized actin cytoskeleton was clearer in Bbs8-deficient 3T3 cells and primary fibroblasts (Fig. 3 *L–O*). These cells showed severe lack of polarization of the cytoskeleton. In scratch wound-healing assays, migration was reduced in mutants of both cell types, compared with controls (Fig. 3 *P–S*).

Aberrant Noncanonical Wnt Signaling May Underlie the Migration Phenotype. Early NCC migration is regulated by noncanonical Wnt signaling (17). Up- and down-regulation of noncanonical Wnt signaling both inhibit NC migration (17). In view of prior evidence of involvement of BBS proteins in this pathway (16), we tested whether this role might extend to NCCs.

We induced noncanonical Wnt signaling in zebrafish by expressing a truncated form of Dishevelled (*Dvl*Δ*N*) (18). At 20ss, embryos injected with *Dvl*Δ*N* showed inhibition of migrating streams of NCCs from the NT (*crestin in situ*; Fig. 4 *A* and *B*). Injection of *bbs8* MO also inhibited migration (Fig. 4*C*). However, coinjecting 3 ng of bbs8 MO and *Dvl*Δ*N* mRNA partially rescued the NCC migration defect (Fig. 4*D*). This rescue was dose-dependent because injection of 2 ng of *bbs8* MO failed to rescue the migration defect (Fig. 4*E*).

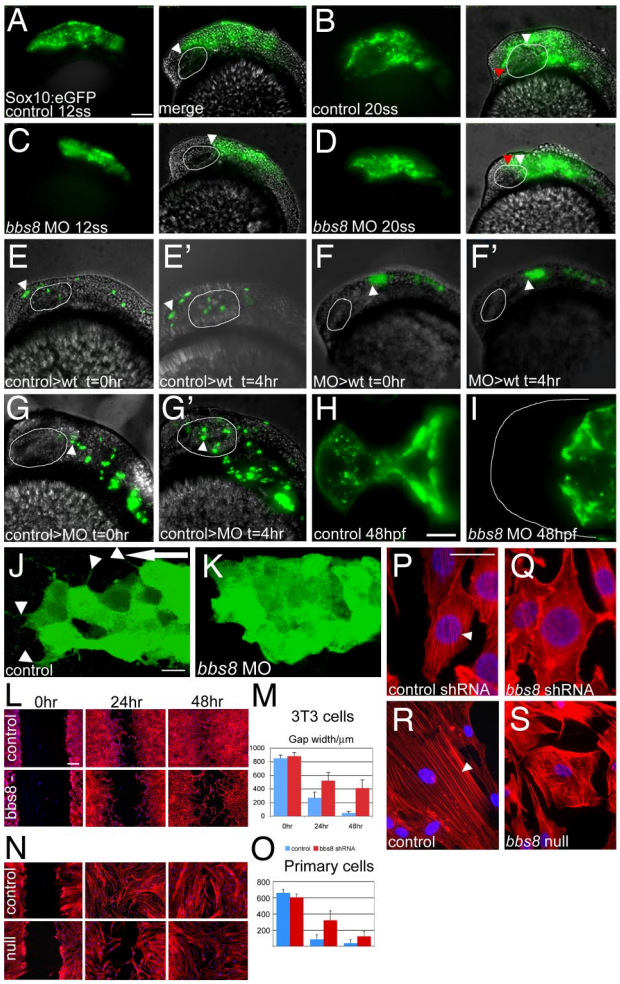

Fig. 3. Neural crest migration in *bbs8* morphants. (*A* and *B*) Sox10:GFP transgenic zebrafish showing migration of CNCCs anteriorly between 12 (*A*) and 20ss (*B*). The amount of movement over the 4-h period is represented in *B* by the difference between the white (position at 12ss) and red (position at 20ss) arrowheads, ≈250 μm. (*C* and *D*) Inhibition of CNCC migration in *bbs8* morphants. Only a small distance (80 μm) moved in the 4-h period. (*E* and *E′*) NCCs from control MO-injected embryos grafted into control hosts migrate anteriorly to populate the head. The arrowhead shows the position of the anteriormost cell showing its change in position over the 4-h period. (*F* and *F′*) Cells taken from *bbs8* morphant donors fail to migrate when transplanted into control hosts, suggesting that the migration defect is cell autonomous. (*G* and *G′*) Control cells transplanted into *bbs8* morphant hosts migrate as normal. (*H* and *I*) Control and morphant embryos at 48 hpf showing Sox10:eGFP expression in the developing trabeculae that fail to elongate in morphants. (*J*) Migrating control CNCCs at 14ss showing polarized filopodial protrusions (arrowheads) mainly in the direction of migration (large arrow). (*K*) *bbs8* morphant CNCCs remain tightly clustered and lack polarized protrusions. (*L*) *In vitro* scratch wound healing assay on 3T3 cells shows delayed closure of the gap in Bbs8 knockdown cells compared with controls. (*M*) Graph quantifying the gap width over the 48-h time course. (*N*) The same wound healing assay using primary fibroblasts taken from unaffected and *BBS8*$^{-/-}$ patients also shows delayed migration. (*O*) *BBS8* patient cells migrate slower than control. (*P*) Polarized actin microfilaments in control 3T3 cells migrating into the wound gap. (*Q*) Bbs8 knockdown cells have a disordered actin cytoskeleton. (*R* and *S*) This disorder is recapitulated in migrating patient primary fibroblasts. [Scale bars: 100 μm (*A–G′*), 100 μm (*H* and *I*), 20 μm (*J* and *K*), 200 μm (*L* and *N*), and 20 μm (*P–S*).]

We confirmed these results by injecting a membrane-targeted Dvl construct (*myr/pal Dvl*) (19), which also caused inhibition of migration, and again was partially rescued by coinjection with 3 ng of *bbs8* MO (Fig. 4 *F* and *G*). Together, these results suggest that perturbation of the noncanonical Wnt pathway may contribute to the NC migration inhibition.

Lack of Enteric Neurons in Morphants Results in Gut Motility Defects. Considering the observed role for Bbs8 in trunk and cranial NC migration, we next investigated whether it had a role in ENS development. This question is pertinent in light of the published association of BBS with HD, a failure of enteric neurons to populate the hindgut.

We examined ENS colonization of the gut using the neuronal marker HuC/HuD. In control larvae at 4 dpf enteric neurons populated the entire length of the gut to the anus (Fig. 5*A*). In *bbs8* morphants (2 ng), these cells extended halfway along the hindgut, never reaching the anus (Fig. 5*B*). With 4 ng of MO, neurons failed to enter the hindgut (Fig. 5*C*). The quantity of neurons in the region between the anus and the start of the yolk stalk was reduced from 108 in controls to 22 and 5 in 2 ng of, and 4 ng of, MO-injected embryos, respectively ($n = 10$ in all cases; $P < 0.001$ for morphants) (Fig. 5*D*).

To investigate the cause of this phenotype, we examined a time course of vagal NC migration. At 36 hpf, NCCs have migrated out of the vagal region normally in *bbs8* morphants, as shown by *crestin* expression (Fig. 5 *E* and *F*). At 48 hpf, *phox2b* expression shows a reduction in the number of cells in the branchial arches (explaining the lack of branchial arches in *bbs8* morphants)(Fig. 5 *G* and *H*). A lateral view shows that there are no cells migrating into the gut tube in morphants at this time (Fig. 5 *I* and *J*), suggesting that the lack of ENS arises from a failure of cells to migrate from the vagal region, through the arches and into the gut, not from a failure of specification or exit from the vagal region.

We confirmed the HuC results by *in situ* hybridization for *phox2b* at 72 hpf. In controls, *phox2b*-positive cells populated the gut to the anus (Fig. 5*K*). With 2 ng of MO, cells reach the midpoint of the hindgut (Fig. 5*L*) whereas higher doses (4 ng of MO) resulted in absence of *phox2b*-positive cells from the hindgut (Fig. 5*M*).

Because GI motility is correlated with enteric neuron numbers, we used video microscopy to observe the mid-intestine in larvae at 4.5 dpf. In all morphants (2 ng of MO), we observed lack of peristalsis correlating with the paucity of enteric neurons (Movies S4 and S5). These data indicate that Bbs8 is important for enteric nervous system population by NCCs migrating from the vagal region and likely explains the association of HD with cases of BBS.

Hedgehog Signaling Is Perturbed in *bbs* Morphant Fish. Finally, we investigated a possible mechanism for the mispatterning of the craniofacial region in *bbs* morphants. Fusion of the trabeculae in *bbs8* morphant embryos, together with partial cyclopia (Fig. 2*D Inset*), was reminiscent of Shh pathway mutants or cyclopamine-treated fish embryos (12). The two main cartilages of the larval ANC, the ethmoid plate and trabeculae (Fig. 2*N*; arrowhead), arise from distinct NCC precursors, and both depend on Shh signaling for their development (14). Notably, BBS patients have polydactyly and hypogenitalism, as well as a low incidence of corpus callosum defects and single central incisor (personal observation), hallmarks of aberrant SHH signaling.

During migration, Shh directs migration and patterning of NCCs (12). Studies in zebrafish and chick indicate that Shh from the facial ectoderm promotes maxillary and frontonasal outgrowth (12). We investigated Shh signaling in *bbs* morphant zebrafish. *Patched1* (*ptc1*), itself a transcriptional target of Shh signaling, is a reliable marker for cellular responses to Shh (20). In 24-hpf morphant embryos, there was an overall reduction in *ptc1* expression in all morphants relative to controls, most striking in *bbs8* (64% reduction by qRT-PCR) (Fig. S8 *A–D*). qRT-PCR also showed Gli1 to be down-regulated to 52% of control expression in *bbs8* morphants. By contrast, the transcription factor *pax6*, normally repressed by Shh signaling, was up-regulated and ectopically expressed throughout the neural tube in *bbs8* morphants (Fig. S8 *E–H*) (21), signifying misregulation of Shh signaling.

Injection of *ptc1* MO (or *shh* mRNA; data not shown) induced the Shh pathway (Fig. S8*I*), and coinjection with *bbs8* MO partially

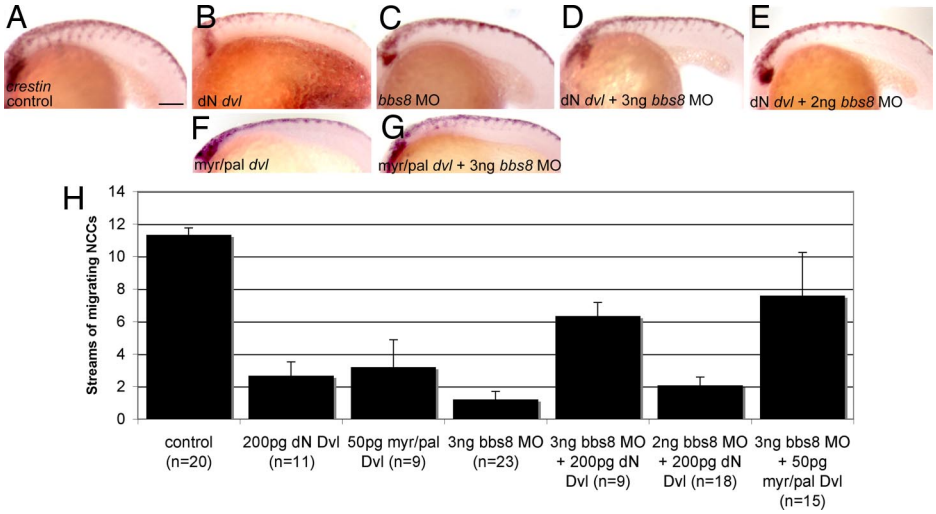

Fig. 4. Noncanonical Wnt signaling and NC migration. (*A–C*) Injection of both *dN dvl* mRNA and *bbs8* MO individually results in inhibition of NCC migration relative to controls. (*D*) Coinjection of 3 ng of *bbs8* MO with *dN dvl* results in partial rescue of NCC migration by ≈4-fold relative to *bbs8* morphants. (*E*) Coinjection of *dN dvl* mRNA with 2 ng of *bbs8* MO fails to rescue NCC migration. (*F*) Injection of 50 pg of *myr/pal dvl* causes inhibition of NCC migration. (*G*) Coinjection of *myr/pal dvl* with 3 ng of *bbs8* MO also partially rescues the inhibited NC migration. (*H*) Graph quantifying the number of streams of *crestin*-positive NCCs migrating through the trunk. (Scale bar: 200 μm.)

rescued this induction (Fig. S8*J*), indicating that Bbs8 functions downstream of Ptc1 but is not essential for Shh transduction.

IFT proteins are required for both Gli transcriptional activator and repressor functions, and Gli proteins are insensitive to Hh ligand in the absence of IFT proteins. We tested whether Bbs8 regulates Gli processing in mammalian cells. Adding the Shh agonist Purmorphamine to NIH 3T3 cells stimulates the Shh pathway by directly agonizing Smoothened. Response to stimulation in shRNA-mediated knockdown of Bbs8 was attenuated by ≈40% ($P < 0.01$) (Fig. S8*M*). Western blot analysis for Gli3A:Gli3R ratios in these cells revealed blunted responses to Shh stimuli (Fig. S8 *N* and *O*). This was confirmed *in vivo* by coinjecting zebrafish embryos with a dominant negative PKA mRNA (which disrupts Gli3 phosphorylation); *bbs8* mRNA rescued the phenotype (Fig. S8 *K* and *L*). These results indicate that bbs8 is important, but not essential, for Hh signaling by acting downstream of Ptc1 and in regulating Gli3 processing.

Neural Crest Cells Bear Primary Cilia. Considering the importance of cilia for Shh and noncanonical Wnt signaling, that Shh is essential for midline guidance of migrating CNCCs, and the role of noncanonical Wnt in NCC migration, we reasoned that migrating NCCs should bear primary cilia with which they sense morphogen gradients and possibly regulate cell polarity (14, 17, 22). After fluorescence microdissection of Sox10:eGFP NCCs, we observed clear apical primary cilia (stained with acetylated tubulin) consistent with the requirement for cilia-dependent Shh transduction (Fig. S9 *A*, *B*, and *B′*).

We confirmed that Shh was not important for early NCC migration by antagonizing Shh signaling using cyclopamine. CNCCs still migrated normally at 19 hpf even though patterning was disrupted by 30 hpf (Fig. S10).

Discussion

In this study, we have shown that DSM analysis can be used effectively to define subtle facial dysmorphism in both humans and mouse. DSM can highlight key differences in the facies of genetic conditions such as Smith-Magenis syndrome, Velo-cardio-facial syndrome, Williams syndromes, and now BBS (2, 3).

The advantages of using DSM analysis of BBS facial morphology over reliance on human observation are objectivity and the ability to adjust for size so that observed mid-facial patterning is not dominated by excessive facial tissue. We can now ascertain maxillary flattening with on average a smaller nose and mild retrognathia providing a previously undescribed objective means of facial recognition in BBS (Movie S1). Recent discrimination analyses of the

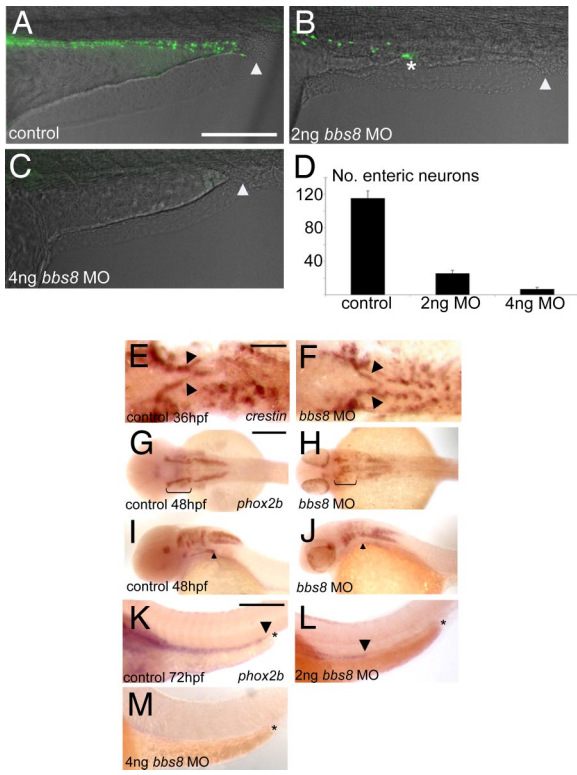

Fig. 5. Enteric nervous system development in bbs morphants. (*A*) Control embryos at 4 dpf showing enteric neurons populating the length of the gut from the anterior (left-hand side) to the anus (arrowhead). (*B*) With 2 ng of *bbs8*, MO migration of enteric neurons ceases midway along the gut (asterisk), and no neurons reach the anus (arrowhead). (*C*) Four nanograms of *bbs8* MO causes complete absence of enteric neurons, resulting in gut motility defects (see Movie S4 and Movie S5). (*D*) Quantification of the reduction in number of enteric neurons with progressively higher doses of *bbs8* MO. (*E* and *F*) NCCs exiting the vagal region visualized by *crestin* show no difference between control and morphant. (*G* and *H*) *phox2b* expression at 48 hpf shows a reduced number of NCCs in the branchial arches. (*I* and *J*) Lateral view of the embryos in *G* and *H* shows a failure of cells to leave the pharyngeal arches and enter the gut tube. (*K*) *phox2b*-positive enteric neurons populating the entire length of the gut all the way to the anus. The arrowhead shows the posteriormost extent of migration, and the asterisk represents the anus. (*L* and *M*) Injection of 2 ng of, and 4 ng of, *bbs8* MO, respectively, causes neurons to migrate only halfway along the gut (2 ng) or fail to enter the gut at all (4 ng). [Scale bars: 500 μm (*A–D*), 100 μm (E and F), 200 μm (*G–J*), and 300 μm (*K–M*).]

faces of controls and matched individuals with genetic conditions have performed at accuracy levels of between 85% and 95% (2), and now the nasal region alone in BBS offers similar accuracy. We also extended DSM-based analysis to mice and demonstrated comparable craniofacial abnormalities in mouse, as well as fish, models of BBS. These results suggest that BBS genes have a crucial role in CF development.

Despite morphological differences between human, mouse, and fish skulls, many of the same signaling pathways and embryological sequences regulate their CF development (12). The zebrafish has become a valid model for the study of CF development (14). Similar to previously reported zebrafish models of human genetic diseases, observed phenotypes are often more pronounced likely because of the rapid development and associated sensitivity to genetic perturbation (23, 24).

We have observed defective development in comparable skeletal regions of the mid-face in both mouse and humans mutated for BBS genes. In fish, we identified a requirement of Bbs8 for CNCC migration in to the anterior section of the head. Shh-like craniofacial defects in *bbs8* morphants have led us to demonstrate that Bbs proteins are also required for efficient Shh signaling. In light of recent studies indicating the importance of cilia and IFT in successful Shh transduction (22, 25, 26) and knowledge that Bbs proteins regulate IFT processes (5, 27), BBS deficiency can explain the craniofacial dysmorphology.

These migratory defects were not confined to CNCCs: we showed a lack of ENS development and loss of gut motility in Bbs morphants probably explaining the association of HD with BBS (8, 28, 29). HD arises as a consequence of NCC migration defects and has been linked to Hh deregulation. *Shh* mutant mice develop aganglionic colons and anorectal malformations (30, 31), and, moreover, HD has been associated with distal limb defects, anorectal malformations, and HPE (11).

Although early NC migration is Shh-independent, we show that it may depend, at least in part, on noncanonical Wnt signaling. Therefore, we propose a hypothesis for the development of CF dysmorphology and HD whereby a lack of BBS proteins perturbs noncanonical Wnt signaling essential for early NCC migration. Because Shh signaling in CNCCs is essential for normal patterning (12), we speculate that NCCs arriving in the head have a depressed response to Shh secreted by the facial ectoderm, culminating in poor maxillary and frontonasal outgrowth. The combination of inhibition of migration and Shh insensitivity in Bbs-deficient NCCs provides a mechanism for development of aganglionic segments in BBS-associated HD.

Methods

Human and Mouse Craniofacial Study. BBS patients and unaffected controls were subjected to 3D facial scanning, and the ''mean'' face was calculated. *Bbs4*$^{-/-}$ and WT mouse fur was painted with cornstarch and scanned for gross facial morphology. Skulls were prepared by using potassium hydroxide and scanned on a benchtop laser scanner. Dense surface morphometry was compiled by using in-house custom software.

Zebrafish. Morpholinos against *bbs4*, *bbs6*, and *bbs8* were injected into zebrafish embryos. For wholemount *in situ* hybridization, standard protocols were used with the following probes: *ptc1*, *pax6*, *phox2b*, *foxd3*, *sox10*, and *crestin*. Immunohistochemistry was performed by using standard protocols. Embryos were imaged on a Leica SPUV confocal microscope. For FACS analysis, embryos were dissociated with trypsin and triturated before sorting with a Beckton Dickinson FACS machine.

Cell Culture. NIH 3T3 cells stably expressing an shRNA against *bbs8* or control sequence were stimulated with purmorphamine (Calbiochem) or recombinant Shh (R & D Systems) and subjected to a luciferase assay (Promega). Alternatively, cells were lysed, and the proteins were electrophoresed and blotted with anti-Gli3 antibody (Santa Cruz). For wound healing assays, a scratch was made on cultured NIH 3T3 or primary human fibroblasts. The actin cytoskeleton was stained with Phalloidin-594 (Invitrogen) and imaged on a Zeiss AxioImager. Full materials and methods can be found in *SI Materials and Methods*.

ACKNOWLEDGMENTS. We thank all the patients and members of the Laurence-Moon-Bardet-Biedl Society who took part in the facial scanning study; Masatake Kai (University College London) and Anita Mynett (National Institute for Medical Research, London) for technical support and reagents; Dan Jagger for help with confocal imaging; Robert Kelsh (University of Bath, Bath, U.K.) for the gift of Sox10:GFP fish; Peter Scambler for helpful commentary; and Nico Katsanis (The Johns Hopkins University, Baltimore) for the gift of *bbs4* and *-6* morpholinos. This work was supported by the National Institutes of Health (NIH) (M.D.F.); was partially supported by NewLife (Birth Defects Foundation) and by NIH Grants P50 DE 016215-01 and Fogarty/NIH R21TW06761-01 (to P.H.); was supported in part by the National Institute of Dental and Craniofacial Research, NIH Grant RO1 DE015210 (to J.R.L.); was supported by NIH Grants P01 ES11253 and R01 HD39372 (to M.J.J.); and was supported by the Medical Research Council (J.L.T., J.B., and H.M.-S.). P.L.B. is a Wellcome Trust Senior Research Fellow.

1. Winter RM (1996) Analysing human developmental abnormalities. *Bioessays* 18:965–971.
2. Hammond P, *et al*. (2005) Discriminating power of localized three-dimensional facial morphology. *Am J Hum Genet* 77:999–1010.
3. Tassabehji M, *et al*. (2005) GTF2IRD1 in craniofacial development of humans and mice. *Science* 310:1184–1187.
4. Tobin JL, Beales PL (2007) Bardet-Biedl syndrome: Beyond the cilium. *Pediatr Nephrol* 22:926–936.
5. Ansley SJ, *et al*. (2003) Basal body dysfunction is a likely cause of pleiotropic Bardet-Biedl syndrome. *Nature* 425:628–633.
6. Kim JC, *et al*. (2004) The Bardet-Biedl protein BBS4 targets cargo to the pericentriolar region and is required for microtubule anchoring and cell cycle progression. *Nat Genet* 36:462–470.
7. Kim JC, *et al*. (2005) MKKS/BBS6, a divergent chaperonin-like protein linked to the obesity disorder Bardet-Biedl syndrome, is a novel centrosomal component required for cytokinesis. *J Cell Sci* 118:1007–1020.
8. Beales PL, Elcioglu N, Woolf AS, Parker D, Flinter FA (1999) New criteria for improved diagnosis of Bardet-Biedl syndrome: Results of a population survey. *J Med Genet* 36:437–446.
9. Lorda-Sanchez I, Ayuso C, Sanz R, Ibanez A (2001) Does Bardet-Biedl syndrome have a characteristic face? *J Med Genet* 38:E14.
10. Moore SJ, *et al*. (2005) Clinical and genetic epidemiology of Bardet-Biedl syndrome in Newfoundland: A 22-year prospective, population-based, cohort study. *Am J Med Genet A* 132:352–360.
11. Amiel J, Lyonnet S (2001) Hirschsprung disease, associated syndromes, and genetics: A review. *J Med Genet* 38:729–739.
12. Tapadia MD, Cordero DR, Helms JA (2005) It's all in your head: New insights into craniofacial development and deformation. *J Anat* 207:461–477.
13. Burns AJ, Thapar N (2006) Advances in ontogeny of the enteric nervous system. *Neurogastroenterol Motil* 18:876–887.
14. Wada N, *et al*. (2005) Hedgehog signaling is required for cranial neural crest morphogenesis and chondrogenesis at the midline in the zebrafish skull. *Development* 132:3977–3988.
15. Badano JL, *et al*. (2006) Dissection of epistasis in oligogenic Bardet-Biedl syndrome. *Nature* 439:326–330.
16. Ross AJ, *et al*. (2005) Disruption of Bardet-Biedl syndrome ciliary proteins perturbs planar cell polarity in vertebrates. *Nat Genet* 37:1135–1140.
17. De Calisto J, Araya C, Marchant L, Riaz CF, Mayor R (2005) Essential role of noncanonical Wnt signalling in neural crest migration. *Development* 132:2587–2597.
18. Tada M, Smith JC (2000) Xwnt11 is a target of *Xenopus Brachyury*: Regulation of gastrulation movements via Dishevelled, but not through the canonical Wnt pathway. *Development* 127:2227–2238.
19. Simons M, *et al*. (2005) Inversin, the gene product mutated in nephronophthisis type II, functions as a molecular switch between Wnt signaling pathways. *Nat Genet* 37:537–543.
20. Goodrich LV, Milenkovic L, Higgins KM, Scott MP (1997) Altered neural cell fates and medulloblastoma in mouse patched mutants. *Science* 277:1109–1113.
21. Briscoe J, *et al*. (1999) Homeobox gene Nkx2.2 and specification of neuronal identity by graded Sonic hedgehog signalling. *Nature* 398:622–627.
22. Liu A, Wang B, Niswander LA (2005) Mouse intraflagellar transport proteins regulate both the activator and repressor functions of Gli transcription factors. *Development* 132:3103–3111.
23. Jopling C, van Geemen D, den Hertog J (2007) Shp2 knockdown and Noonan/LEOPARD mutant Shp2-induced gastrulation defects. *PLoS Genet* 3:e225.
24. Li YX, *et al*. (2007) Fetal alcohol exposure impairs Hedgehog cholesterol modification and signaling. *Lab Invest* 87:231–240.
25. Corbit KC, *et al*. (2005) Vertebrate Smoothened functions at the primary cilium. *Nature* 437:1018–1021.
26. Huangfu D, Anderson KV (2005) Cilia and Hedgehog responsiveness in the mouse. *Proc Natl Acad Sci USA* 102:11325–11330.
27. Blacque OE, *et al*. (2004) Loss of *C. elegans* BBS-7 and BBS-8 protein function results in cilia defects and compromised intraflagellar transport. *Genes Dev* 18:1630–1642.
28. de Pontual L, *et al*. (2007) Epistatic interactions with a common hypomorphic Ret allele in syndromic Hirschsprung disease. *Hum Mutat* 28:790–796.
29. Lorda-Sanchez I, Ayuso C, Ibanez A (2000) Situs inversus and hirschsprung disease: Two uncommon manifestations in Bardet-Biedl syndrome. *Am J Med Genet* 90:80–81.
30. Mo R, Kim JH, Zhang J, Chiang C, Hui CC, Kim PC (2001) Anorectal malformations caused by defects in sonic hedgehog signaling. *Am J Pathol* 159:765–774.
31. Ramalho-Santos M, Melton DA, McMahon AP (2000) Hedgehog signals regulate multiple aspects of gastrointestinal development. *Development* 127:2763–2772.